Reconstruction of Delayed Neutron Precursor Groups from Data

Luke Seifert,[*,a] Benjamin Betzler,[a] William Wieselquist,[b] Matthew Jessee,[b]
Madicken Munk,[a,c] and Kathryn Huff[a]

[a] *Advanced Reactors and Fuel Cycles Group, University of Illinois at Urbana-Champaign 104 S Wright St, Urbana, IL 61801*

[b] *Nuclear Energy and Fuel Cycle Division, Oak Ridge National Laboratory, Oak Ridge, TN 5200, 1 Bethel Valley Rd, Oak Ridge, TN 37830*

[c] *School of Nuclear Science and Engineering, Oregon State University, Corvallis, OR 211 Merryfield Hall, Corvallis, OR 97331*

[*]Email: seifert5@illinois.edu

Number of pages: 33
Number of tables: 6
Number of figures: 12

Abstract

Delayed neutron precursor (DNP) group data are important for modeling reactor dynamics. Although the data for individual DNPs has been developed over time, the DNP group data present in the Evaluated Nuclear Data Files (ENDF) has not been updated in the past 20 years. In this work, we use SCALE to recreate the Godiva experiment that was used to generate the original DNP group structure for fast fission of ^{235}U. However, each DNP is modeled using up-to-date data, and the results are then converted into a newly updated group structure. This conversion uses an iterative linear least squares solver to minimize chi-squared. The approaches used in this work also enable energy spectrum generation and uncertainty tracking. The method used in this paper for fast ^{235}U fission DNP group structure updating can be applied to different energies and fissile nuclides. Demonstration of the uncertainty tracking in reactor kinetics and dynamics simulations are shown using point reactor kinetics simulations.

Keywords — Delayed Neutron Precursors, ORIGEN, SCALE, ENDF, Precursor Group Parameters

I. INTRODUCTION

Delayed neutron precursors (DNPs) are fission products that are beta-emitting and have sufficient energy to concurrently emit a neutron. (DNPs) are important, as they make reactor control possible. This is due to the time delay which occurs before a delayed neutron is emitted. Thus, the time delay is based on the half-life of the beta emission. Additionally, some isotopes have sufficient energy to emit multiple neutrons, each of which has different probabilities of occurring.

For many reactor kinetics and dynamics simulations, the DNPs are not all explicitly modeled. Instead, it is computationally practical to divide the DNPs into six to eight groups per fissile isotope. Each of these groups has both a half-life and a yield, or abundance. The half-life of the group is based on the half-lives of the constituent DNPs in that group, while the abundance is based on the amount of DNPs in that group and the average number of neutrons they emit. The differences in group half-lives and abundances between different fissile nuclides are caused by fission yield differences. These yield differences affect the specific DNP concentrations, thus affecting the DNP group parameters that are calculated.

The International Atomic Energy Agency (IAEA) maintains a database of DNP data, which has updated data as recent as 2020 and was last updated in 2022 [1]. Although these more recent IAEA data exist, the DNP group data used in the Evaluated Nuclear Data File (ENDF)/B-VIII.0 library have not been updated since ENDF/B-VI.8 [2], approximately 20 years ago [3]. Additionally, the spectral data have not been updated in ∼30 years [4, 5]. This work reconstructs the DNP groups using recent data to evaluate whether the group yield and decay parameters must be altered, or if current parameters are sufficient.

II. METHODS

DNP group data have historically been generated either experimentally, referred to as the macroscopic approach, or computationally, referred to as the microscopic approach, by counting the delayed neutrons after irradiation [6, 7, 5, 8, 9, 3]. For the macroscopic approach, a fissile sample is irradiated, and the delayed neutron counts are collected. For the microscopic approach, data on individual DNPs is used to simulate a delayed neutron count curve. In this work, the microscopic approach is used.

Following the generation of delayed neutron counts over time, both approaches then use the same methodologies to generate DNP group parameters. In this work, the primary difference in the generated DNP group parameters comes from the data used for the individual DNPs. This work proposes a new method for generation of DNP group spectral fits, as the DNP group parameter fitting methodology employed in this work enables spectrum fitting as a straightforward extension. The previous approaches for generating these DNP group spectra are improved by allowing DNP group spectra to contribute to every DNP group rather than only two groups [10, 11, 5, 12, 13]. This work also shows how the DNP group parameters from different data compare when used in a point kinetics model. The uncertainties are tracked throughout, as the more recent individual DNP data have uncertainties which can be propagated.

To use the microscopic approach, it is necessary to simulate the irradiation of a sample. The tools used in this work are in-house Python scripts and SCALE 6.3, within which TRITON and ORIGEN were used for most of the analysis. TRITON is a reactor physics and depletion sequence, and ORIGEN is a depletion and decay solver [14]. Specifically, the "T6-DEPL" TRITON sequence was used that enables TRITON to run with KENO-VI as neutron transport. These tools combined allow a reactor to be modeled, within which a sample can be irradiated. The composition of the sample can then be extracted and allowed to decay over time. POLARIS, which handles light water reactor lattice physics, was used for comparing the different DNP group fits after the results were generated.

The primary model of interest in this work is Godiva, a uniform sphere of ^{235}U with a diameter of $6\frac{3}{4}$ inches and density of 19 g/cm^3 [15]. Godiva is selected as the model of interest to replicate the experimental approach used by Keepin, Wimett, and Zeigler [6]. An additional model considered is a generic Westinghouse 17×17 pressurized water reactor (PWR), though the Godiva model is given more attention in this work. The PWR model is used to understand the impact of the uncertainties and altered DNP group parameters. The TRITON input deck generated a Godiva geometry and imparted a $0.25ms$ pulse irradiation with roughly 10^{16} fission events. The Godiva sphere does not deplete, but rather a 3 gram sample within Godiva is irradiated, the same as in the Keepin, Wimett, and Zeigler experiment [6]. The irradiation was then followed by a $330s$ decay of the sample using logarithmically spaced time nodes to capture the short-lived DNPs' response in ORIGEN. This method replicated the one used by Keepin, Wimett, and Zeigler so that the results

could be directly compared [6]. In the Keepin, Wimett, and Zeigler experiment, the data of interest used for analysis is the delayed neutron count over time.

Using data from the Godiva simulation and recently published experimental data, the delayed neutron count can be constructed. Equation (1) shows how the data comes together to form the delayed neutron count, n_d. This equation sums over all DNPs, I, (the number of which can vary based on the dataset), and calculates the time dependent delayed neutron count from each. This contribution from each DNP is then multiplied by the efficiency of the neutron detector, ϵ. The detector efficiency term is set to 3.75×10^{-8} to scale the delayed neutron count profile to the results from Keepin, Wimett, and Zeigler [6]. Adjusting the efficiency term changes the delayed neutron count rate scaling, but does not affect the generated group fits themselves.

$$n_d(t) = \epsilon \sum_{i=1}^{I} P_{n_i} \lambda_i N_i(t). \tag{1}$$

The concentration of each DNP in atoms, $N_i(t)$, can be retrieved from the ORIGEN binary concentration file. These can then be combined with the emission probabilities, $P_{n,i}$, and decay constants, λ_i, from the IAEA database to generate the neutron emission rate as a function of time. This can then be multiplied by the detector efficiency term, ϵ, to generate the delayed neutron count.

The delayed neutron count rate, $n_d(t)$ can be determined in two different ways using the previously described methodology. The first, called *IAEA–ORIGEN* in subsequent sections, is using ORIGEN to calculate $N_i(t)$ and IAEA emission probabilities, P_{n_i}, and decay constants, λ_i, to calculate $n_d(t)$. The second, called *Pure ORIGEN* in subsequent sections, is by reading $n_d(t)$ directly from the ORIGEN output, where ORIGEN uses a modified ENDF/B-VII.0 dataset for emission probabilities and decay constants. More specifically, the Pure ORIGEN delayed neutron count rate uses SCALE 6.2.4 neutron emission, which uses an embedded version of SOURCES4C, a code system that determines neutron production rates and spectra, combined with a modified ENDF/B-VII.0 dataset [16]. In some cases, IAEA-ORIGEN may require data to supplement the IAEA database. When this occurs, the IAEA-ORIGEN approach obtains data from the Evaluated Nuclear Structure Data File (ENSDF) and ENDF/B-VIII.1 to fill in gaps between the datasets [17, 2].

II.A. Group Parameter Fitting

Generation of the DNP group parameters requires generation of the group yield, a_g, and group decay constant, λ_g, for each group. To generate these parameters, this work uses an iterative least squares approach. For a pulse irradiation with n DNP groups and m time nodes, Equations (3)–(7) show how the iterative least squares problem is configured for Equation (2). The explicitly formatted pulse irradiation least squares problem is given as

$$n_d(t) \approx \epsilon F_s \sum_{g=1}^{n} a_g \lambda_g e^{-\lambda_g t}, \tag{2}$$

which is generalizable to a format one may recall from linear algebra as

$$A\vec{x} \approx \vec{b}. \tag{3}$$

The a_g, also given as $\nu_{d,g}$, values are the group yield, or group abundance, values. These represent the number of delayed neutrons per fission; when summed, they provide the total delayed neutron yield per fission. The F_s value is the total number of fission events that take place within the sample, and ϵ is the detector efficiency. The efficiency of the neutron detector in this work, ϵ, is set so that the Keepin, Wimett, and Zeigler delayed neutron count rate, when using their group yields and decay constants, aligns with the count rate they measured [6]. The total number of delayed neutrons is known by integrating the delayed neutron rate curve. The number of fissions and efficiency term are known as well. The unknowns are the decay constants for each group, λ_g, and the group yields, a_g. For a given set of group decay constants, the problem can be formatted as follows:

$$A = \begin{vmatrix} \lambda_1 e^{-\lambda_1 t_0} & \lambda_2 e^{-\lambda_2 t_0} & \dots & \lambda_n e^{-\lambda_n t_0} \\ \lambda_1 e^{-\lambda_1 t_1} & \lambda_2 e^{-\lambda_2 t_1} & \dots & \lambda_n e^{-\lambda_n t_1} \\ \vdots & \vdots & \ddots & \vdots \\ \lambda_1 e^{-\lambda_1 t_m} & \lambda_2 e^{-\lambda_2 t_m} & \dots & \lambda_n e^{-\lambda_n t_m} \end{vmatrix}, \tag{4}$$

$$\vec{x} = \begin{vmatrix} \nu_{d,1} \\ \nu_{d,2} \\ \vdots \\ \nu_{d,n} \end{vmatrix}, \tag{5}$$

$$\vec{b} = \begin{vmatrix} \frac{n_d(t_0)}{\epsilon F_s} \\ \frac{n_d(t_1)}{\epsilon F_s} \\ \vdots \\ \frac{n_d(t_m)}{\epsilon F_s} \end{vmatrix}, \tag{6}$$

where the solution for the group yields with the given set of group decay constants is:

$$\vec{x} \approx (A^T A)^{-1} A^T \vec{b}. \tag{7}$$

An iterative process is used to modify the group decay constants. The iteration process goes through Equations (3)–(7) for every combination of values in L, an example of which is shown in Equation (8) for a case with three decay constant nodes per DNP group. The values of λ_g are linearly spaced from $(1-\mu)\,\lambda_g$ to $(1+\mu)\,\lambda_g$. The number of iterations for a given value of μ is equal to the number of decay constant nodes to the power of the number of groups. For six DNP groups, this means that to find the optimal set of decay constants, 729 iterations are required for three nodes and 15,625 iterations are required for five nodes.

$$L = \begin{vmatrix} (1-\mu)\,\lambda_1 & \lambda_1 & (1+\mu)\,\lambda_1 \\ (1-\mu)\,\lambda_2 & \lambda_2 & (1+\mu)\,\lambda_2 \\ \vdots & \vdots & \vdots \\ (1-\mu)\,\lambda_n & \lambda_n & (1+\mu)\,\lambda_n \end{vmatrix} \tag{8}$$

Following an iteration for a given value of μ, the values of λ_g are set to the values which minimize chi-squared, as shown in Equation (9). Equations (10) through (13) define the terms used within the chi-squared calculation. Once a new solution is found which has a smaller value for chi-squared, the iteration goes back to the largest value of μ. For example, the values of μ in this work are set to 0.1, 0.05, 0.04, 0.03, 0.02, 0.01, and finally 0.005 to have decay constants resolved

to within 0.5%. Starting with smaller values of μ means that the values of λ_g may take a long time to resolve or fail to find the best fit if the initial guess is far from the global chi-squared minimum. The convergence criteria used is to stop when the smallest value of μ no longer improves the fit.

$$\chi^2 = \sum_{j=1}^{m} \left(\frac{n_{d,j} - \sum_{g=1}^{n} a_g \lambda_g e^{-\lambda_g t_j}}{\Delta n_d(t_j)} \right)^2, \tag{9}$$

$$m = \text{number of time nodes}, \tag{10}$$

$$n = \text{number of precursor groups}, \tag{11}$$

$$n_{d,j} = \text{delayed neutron counts at time } j, \tag{12}$$

$$\Delta n_d(t_j) = \text{uncertainty in delayed neutron count rate at time } j. \tag{13}$$

The uncertainty in the delayed neutron count rate is discussed in Section II.D.

II.B. Spectrum Fitting

Group fits are used for the yield and decay constants, but there is also a desire to have group spectra, χ_g. This is referred to in this work as generating a spectral fit. In the past, the spectral fits were generated by allowing each isotope to contribute some fraction of its spectrum to its closest groups, sorted by group half-life [10, 11, 5] or based on nuclide half-life [12, 13]. This work refers to such approaches as *fractional fitting least squares*. Alternatively, using an iterative least squares technique allows for a more optimal set of group fits such that isotopes can contribute to more than two groups. This method also requires no individualized spectral data for the isotopes, yielding no potential error from erroneous spectral data within the fitting method. This method is referred to as *iterative least squares* in this work.

To determine the energy spectrum of neutrons emitted by each precursor group, the delayed neutron emission rate as a function of time and energy, $n_d(E,t)$, can either be collected from the ORIGEN output or generated from the IAEA database using Equation (14):

$$n_d(E,t) = \epsilon \sum_{i=1}^{I} \chi_i(E)\lambda_i N_i(t) P_{n_i}. \tag{14}$$

In this equation, I represents the total number of DNPs. Once the two-dimensional set of values for $n_d(E,t)$ is collected, the group spectra are generated using iterative least squares. This method iterates through each possible energy bin while solving the least squares problem for every time node, thus optimizing every j^{th} energy bin for all times. Equations (15)–(18) show the iterative least squares method used, whereas Equations (19) and (21) show the solutions using ordinary least squares and using the percent regression least squares, respectively [18]:

$$n_d(E,t) \approx \epsilon F_s \sum_{g=1}^{n} \chi_g(E)\lambda_g a_g e^{-\lambda_g t}, \tag{15}$$

$$A = \begin{vmatrix} \lambda_1 \nu_{d,1} e^{-\lambda_1 t_0} & \lambda_2 \nu_{d,2} e^{-\lambda_2 t_0} & \dots & \lambda_n \nu_{d,n} e^{-\lambda_n t_0} \\ \lambda_1 \nu_{d,1} e^{-\lambda_1 t_1} & \lambda_2 \nu_{d,2} e^{-\lambda_2 t_1} & \dots & \lambda_n \nu_{d,n} e^{-\lambda_n t_1} \\ \vdots & \vdots & \ddots & \vdots \\ \lambda_1 \nu_{d,1} e^{-\lambda_1 t_m} & \lambda_2 \nu_{d,2} e^{-\lambda_2 t_m} & \dots & \lambda_n \nu_{d,n} e^{-\lambda_n t_m} \end{vmatrix}, \tag{16}$$

$$\vec{x} = \begin{vmatrix} \chi_1(E_j) \\ \chi_2(E_j) \\ \vdots \\ \chi_n(E_j) \end{vmatrix}, \tag{17}$$

$$\vec{b} = \begin{vmatrix} \frac{n_d(E_j,t_0)}{\epsilon F_s} \\ \frac{n_d(E_j,t_1)}{\epsilon F_s} \\ \vdots \\ \frac{n_d(E_j,t_m)}{\epsilon F_s} \end{vmatrix}, \tag{18}$$

$$\vec{x} \approx (A^T A)^{-1} A^T \vec{b}, \tag{19}$$

It follows the percentage regression least squares formulation to take the inverse of $\vec{b}$ and form a diagonal matrix to solve Equation (19) [18]. This is shown in Equation (20):

$$D = \begin{vmatrix} \frac{\epsilon F_s}{n_d(E_j,t_0)} & 0 & \dots & 0 \\ 0 & \frac{\epsilon F_s}{n_d(E_j,t_1)} & \dots & 0 \\ \vdots & \vdots & \ddots & \vdots \\ 0 & 0 & \dots & \frac{\epsilon F_s}{n_d(E_j,t_m)} \end{vmatrix} \tag{20}$$

We can then solve for $\vec{x}$ using this definition of D as shown in Equation (21):

$$\vec{x} = (A^T D^2 A)^{-1} A^T D^2 \vec{b}. \tag{21}$$

Equation (21) was incorporated into the non-negative least squares method in the outer loop, whereas the residual in the outer loop was adjusted to solve the residual equation shown in Equation (22) [19]:

$$argmin_x \left|\left| \frac{Ax - b}{b} \right|\right|_2. \tag{22}$$

This approach is computationally costly, can calculate a negative group spectrum probability, and can be inaccurate at long times. Although the computational cost issue will remain, the other issues can be solved by implementing a combination of non-negative least squares and least squares percentage regression techniques [19, 18]. However, a solution with a smaller residual as shown in Equation (22) is generated by instead implementing the least squares percentage regression and then setting any negative emission probability bin values to 0.

II.C. Point Reactor Kinetics

Using the point reactor kinetics equations enables an understanding of how the group fits will affect the reactor systems we are modeling. The time rate of change of neutrons in the system is given by:

$$\frac{dn}{dt} = \frac{\rho - \beta}{\Lambda} n(t) + \sum_{g=1}^{6} \lambda_g C_g(t), \tag{23}$$

where:

$$\begin{aligned} \rho &= \text{reactivity}, \\ \beta &= \text{delayed neutron fraction}, \\ \Lambda &= \text{neutron generation time}. \end{aligned} \tag{24}$$

The time rate of change of the group g precursor concentration is given by:

$$\frac{dC_g}{dt} = \frac{\beta_g}{\Lambda} n(t) - \lambda_g C_g(t), \tag{25}$$

where:

$$\beta_g = \text{delayed neutron fraction of group } g. \tag{26}$$

The initial conditions for Equations (23) and (25) are:

$$\begin{aligned} n_0 &= 1, \\ c_{g_0} &= \beta_g n_0 \left(\lambda_g \Lambda\right)^{-1}. \end{aligned}$$

The β_g values are calculated using the group yields, a_g, and average neutron emission per fission event, $\bar{\nu}$, as shown in Equation (42):

$$\beta_g = \frac{a_g}{\bar{\nu}}. \tag{27}$$

In this work, the equations were solved using the forward Euler method, shown in Equations (28) and (29):

$$n^{(m)} = n^{(m-1)} + \frac{dn^{(m-1)}}{dt} \Delta t, \tag{28}$$

$$C_{g^{(m)}} = C_{g^{(m-1)}} + \frac{dC_{g^{(m-1)}}}{dt} \Delta t. \tag{29}$$

The forward Euler method is used in this work because generating and providing results that demonstrate the differences yielded from each data set is simple using this approach. Because the purpose of the point reactor kinetics here is to demonstrate a general trend caused by differences between the DNP group parameters, a more advanced method would introduce more complexity than desired.

II.D. Uncertainties

An important consideration for the group fit methods are the uncertainties in the data used. The DNP group parameter uncertainties have contributions from decay constants, delayed neutron emission counts, and fissions [20]. These uncertainties can be propagated to the DNP group parameters and spectra, which can then be propagated again to the models which use that data. In this work, these uncertainties are propagated through to the point reactor kinetics analysis.

The uncertainty in the delayed neutron emission counts from ORIGEN can be determined based on Equation (1), rewritten here, by using Equations (30)–(33). Equation (1) does not account for decay parents of the DNPs, instead treating the concentration of each as a decay over time from the initial concentration. The partial derivative is taken for each variable with uncertainty, which are the emission probability for DNP i, P_{n_i}; the initial concentration of DNP i before measuring the delayed neutron count rate, N_{0_i}; and the decay constant for DNP i, λ_i. These partial derivatives are then used in the uncertainty calculation in the delayed neutron count from each individual delayed neutron precursor as shown in Equation (33).

$$n_d(t) = \epsilon \sum_{i=1}^{I} P_{n_i} \lambda_i N_{0_i} e^{-\lambda_i t}.$$

This uncertainty is then used in Equations (34)–(37) to calculate the uncertainty for the entire right-hand side of the least squares problem given in Equation (3), rewritten here.

$$A\vec{x} \approx \vec{b}.$$

The uncertainty in the emission probabilities, ΔP_{n_i}, comes from the IAEA data; the uncertainty in concentration, ΔN_{0_i}, comes from Sampler, a SCALE tool that stochastically computes and propagates uncertainties [14]; and the uncertainty in the decay constants, $\Delta\lambda_i$, comes from

the IAEA data for the ORIGEN delayed neutron counts and is based on the mesh for the group fit. Sampler is used with 500 samples, with perturbations in each non-metastable nuclide of cross sections, yields, and decay constants.

$$\frac{\partial n_d(t)}{\partial P_{n_i}} = \lambda_i N_{0_i} e^{-\lambda_i t}, \tag{30}$$

$$\frac{\partial n_d(t)}{\partial \lambda_i} = P_{n_i} N_{0_i} (1 - \lambda_i t) e^{-\lambda_i t}, \tag{31}$$

$$\frac{\partial n_d(t)}{\partial N_{0_i}} = P_{n_i} \lambda_i e^{-\lambda_i t}, \tag{32}$$

$$\begin{aligned} \Delta n_d^2(t) = \epsilon \sum_{i=1}^{n} \left(\frac{\partial n_d(t)}{\partial P_{n_i}} \Delta P_{n_i} \right)^2 + \left(\frac{\partial n_d(t)}{\partial \lambda_i} \Delta \lambda_i \right)^2 \\ + \left(\frac{\partial n_d(t)}{\partial N_{0_i}} \Delta N_{0_i} \right)^2. \end{aligned} \tag{33}$$

With the uncertainty in the delayed neutron counts calculated, the uncertainty in the DNP group parameters is one step closer to being calculated. The next step is to propagate this uncertainty to the linear algebra equation that is used to find the DNP group parameters. Equation (34) is the right-hand side vector at a point in time m used when fitting the group constants. Partial derivatives are taken with respect to the delayed neutron count rate and the number of fissions from Equation (34), shown in Equations (35) and (36). These partial derivatives are then used to generate the uncertainty at that time, shown in Equation (37).

$$\vec{b}_m = \frac{n_d(t_m)}{\epsilon F_s}. \tag{34}$$

$$\frac{\partial \vec{b}_m}{\partial n_d(t_m)} = \frac{1}{\epsilon F_s}, \tag{35}$$

$$\frac{\partial \vec{b}_m}{\partial F_s} = -\frac{n_d(t_m)}{\epsilon F_s^2}, \tag{36}$$

$$\Delta\vec{b}_m = \frac{1}{\epsilon}\sqrt{\left(\frac{\partial\vec{b}_m}{\partial n_d(t_m)}\Delta n_d(t_m)\right)^2 + \left(\frac{\partial\vec{b}_m}{\partial F_s}\Delta F_s\right)^2}. \tag{37}$$

The uncertainty in the delayed neutron emission counts from the group fit can be found using Equations (2) and the partial derivatives in Equations (38)–(39), yielding the result in Equation (40).

$$\frac{\partial n_d}{\partial a_g} = \lambda_g e^{-\lambda_g t}, \tag{38}$$

$$\frac{\partial n_d}{\partial \lambda_g} = a_g(1-\lambda_g t)e^{-\lambda_g t}, \tag{39}$$

$$\Delta n_d(t) = \epsilon F_s\sqrt{\sum_{i=1}^{n}\left(\frac{\partial n_d}{\partial a_g}\Delta a_g\right)^2 + \left(\frac{\partial n_d}{\partial \lambda_g}\Delta\lambda_g\right)^2}. \tag{40}$$

The uncertainty in the group yield values, Δa_g, was calculated stochastically. The least squares problem used to solve for a_g was iterated upon with random variations within uncertainties for the various terms until the point at which a normal distribution formed and the standard deviation could be directly extracted. An example of this approach is shown Figure 1, in which the sixth group yield is $(4.3 \pm 0.4) \times 10^{-4}$ delayed neutrons per fission.

Following the group fit are the point reactor kinetics uncertainties that use forward Euler. The decay constant uncertainty comes from the group fits; the initial uncertainties in both the number of neutrons at the current time, $\Delta n^{(m)}$, and the number of precursors in the i^{th} group, $\Delta C_g^{(m)}$, are zero; and the group and total delayed neutron fraction uncertainties, $\Delta\beta_i$ and $\Delta\beta$, respectively, are given in Equations (41) and (42):

$$\Delta\beta_i = \sqrt{\left(\frac{1}{\bar{\nu}}\Delta a_g\right)^2 + \left(\frac{a_g}{\bar{\nu}^2}\Delta\bar{\nu}\right)^2}, \tag{41}$$

$$\Delta\beta = \sqrt{\left(\sum_{i=1}^{n}\Delta\beta_g^2\right)}. \tag{42}$$

The uncertainty in $n^{(m)}$ from Equation (28), rewritten with the fully expanded derivative in

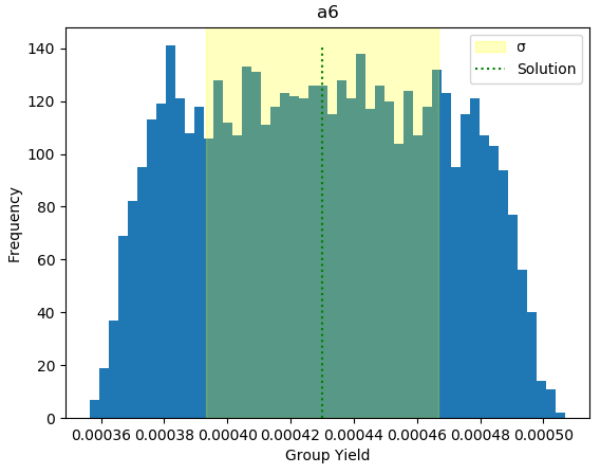

Fig. 1. 5,000 stochastic uncertainty simulations of the Keepin, Wimett, and Zeigler sixth precursor group yield using a μ value of 0.5%.

Equation (43), is given in Equation (49), with the components given in Equations (44)–(48). In these equations, Δt is the time step used in forward Euler:

$$n^{(m)} = n^{(m-1)} + \frac{\rho - \beta}{\Lambda} n^{(m-1)} \Delta t + \sum_{i=1}^{n} \left(\lambda_g C_g^{(m-1)} \Delta t + \frac{\beta_g}{\Lambda} n^{(m-1)} \lambda_g \Delta t^2 - \lambda_g^2 C_g^{(m-1)} \Delta t^2 \right), \tag{43}$$

where the partial derivatives are taken with respect to the previous time step's number of neutrons, $n^{(m-1)}$; decay constant for each group, λ_g; delayed neutron fraction, β; delayed neutron fraction for each group, β_g; and the previous time step's precursor concentration for each group, $C_g^{(m-1)}$. The partial derivatives are given as:

$$\frac{\partial n^{(m)}}{\partial n^{(m-1)}} = 1 + \frac{\rho - \beta}{\Lambda} \Delta t + \sum_{i=1}^{n} \frac{\beta_g}{\Lambda} \lambda_g \Delta t^2, \tag{44}$$

$$\frac{\partial n^{(m)}}{\partial \lambda_g} = C_g^{(m-1)} \Delta t + \frac{\beta_g}{\Lambda} n^{(m-1)} \Delta t^2 - 2 \lambda_g C_g^{(m-1)} \Delta t^2, \tag{45}$$

$$\frac{\partial n^{(m)}}{\partial \beta} = \frac{-n^{(m-1)}\Delta t}{\Lambda}, \tag{46}$$

$$\frac{\partial n^{(m)}}{\partial \beta_g} = \frac{n^{(m-1)}\lambda_g \Delta t^2}{\Lambda}, \tag{47}$$

$$\frac{\partial n^{(m)}}{\partial C_g^{(m-1)}} = \lambda_g \Delta t - \lambda_g^2 \Delta t^2. \tag{48}$$

The partial derivatives are then used to calculate the uncertainty in the number of neutrons at iteration m:

$$\begin{aligned}\left(\Delta n^{(m)}\right)^2 = &\sum_{i=1}^{n} \left(\frac{\partial n(t)}{\partial n^{(m-1)}}\Delta n^{(m-1)}\right)^2 + \left(\frac{\partial n(t)}{\partial \lambda_g}\Delta \lambda_g\right)^2 \\ &+ \left(\frac{\partial n(t)}{\partial \beta}\Delta \beta\right)^2 + \left(\frac{\partial n(t)}{\partial \beta_g}\Delta \beta_g\right)^2 \\ &+ \left(\frac{\partial n(t)}{\partial C_g^{(m-1)}}\Delta C_g^{(m-1)}\right)^2.\end{aligned} \tag{49}$$

The uncertainty in C_g from (29), rewritten with the fully expanded derivative in Equation (50), is given by Equation (55), incorporating the components given by Equations (51)–(54):

$$C_g^{(m)} = C_g^{(m-1)} + \frac{\beta_g}{\Lambda} n^{(m-1)}\Delta t - \lambda_g \Delta t C_g^{(m-1)}, \tag{50}$$

where the partial derivatives are taken with respect to the same variables as the equation for the number of neutrons:

$$\frac{\partial C_g^{(m)}(t)}{\partial C_g^{(m-1)}} = 1 - \lambda_g \Delta t, \tag{51}$$

$$\frac{\partial C_g^{(m)}}{\partial \beta_g} = \frac{n^{(m-1)}\Delta t}{\Lambda}, \tag{52}$$

$$\frac{\partial C_g^{(m)}}{\partial n^{(m-1)}} = \frac{\beta_g \Delta t}{\Lambda}, \tag{53}$$

$$\frac{\partial C_g^{(m)}}{\partial \lambda_g} = -C_g^{(m-1)} \Delta t. \tag{54}$$

The partial derivatives are then used to calculate the uncertainty in each precursor group concentration at iteration m:

$$\begin{aligned}\left(\Delta C_g^{(m)}\right)^2 = \sum_{i=1}^{n} &\left(\frac{\partial C_g^{(m)}}{\partial n^{(m-1)}} \Delta n^{(m-1)}\right)^2 + \left(\frac{\partial C_g^{(m)}}{\partial \lambda_g} \Delta \lambda_g\right)^2 \\ &+ \left(\frac{\partial C_g^{(m)}}{\partial \beta_g} \Delta \beta_g\right)^2 + \left(\frac{\partial C_g^{(m)}}{\partial C_g^{(m-1)}} \Delta C_g^{(m-1)}\right)^2.\end{aligned} \tag{55}$$

Finally, the uncertainty of group spectra constructed using the iterative linear least squares procedure is shown in Equation (56). This uncertainty is fairly straightforward to calculate because the delayed neutron count term, $n_d(t)$, comes from the six group fit for which the uncertainty is given in Equation (40). The uncertainty for the energy-dependent neutron emission counts is shown in Equation (57), where the uncertainty in the spectra, $\Delta\chi_g(E)$, is calculated stochastically, in the same manner as the group yield uncertainties:

$$n_d(E,t) = n_d(t) \sum_g \chi_g(E), \tag{56}$$

$$\Delta n_d^2(E,t) = \left(\Delta n_d(t) \sum_g \chi_g(E)\right)^2 + \left((n_d(t))^2 \sum_g \left(\Delta\chi_g(E)\right)^2\right). \tag{57}$$

III. RESULTS AND ANALYSIS

III.A. ORIGEN Data Compared with IAEA Data

Because the group fits are fit to the delayed neutron count data, it is important to understand how the data compare. The two different datasets compared are the IAEA database and the end7dec default decay ORIGEN library. The end7dec library is referred to as *Pure ORIGEN*, *Pure*, or simply *ORIGEN*, and it uses modified ENDF/B-VII.0 data with an embedded version of SOURCES4C. For analysis of delayed neutron emission counts, the three components that can change from the data source are the time-dependent compositions term, the decay constants term,

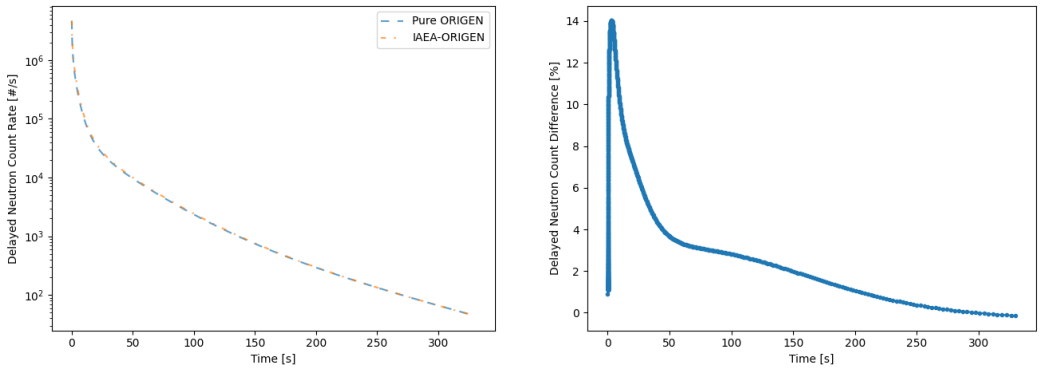

(a) Pure ORIGEN and IAEA ORIGEN count rate over time

(b) Pure ORIGEN and IAEA ORIGEN count rate difference over time normalized by the IAEA ORIGEN count rate

Fig. 2. Comparison of delayed neutron count rate for Pure ORIGEN and IAEA ORIGEN data after fast-pulse irradiation of ^{235}U.

and the emission probabilities term, all of which were first presented in Equation (1).

The composition as a function of time depends on the incident fission neutron energy, the fission yield, the decay constant of the target isotope, and that same data for any isotopes that decay into the target isotope. In this work, the ORIGEN- and IAEA-based data comparisons use the compositions generated by KENO-VI and decayed in ORIGEN.

We can conduct a sensitivity study of the decay constants, λ, and emission probabilities (or branching fractions), P_n, by comparing the results of the Pure ORIGEN dataset simulated in ORIGEN with the IAEA dataset in ORIGEN. Specifically, we can adjust the data such that only decay constants, only emission probabilities, or both are swapped from the Pure ORIGEN dataset values to the IAEA dataset values.

Figure 2 shows the net counts for the Pure ORIGEN and for the IAEA–ORIGEN data sets in which the percent difference of the Pure ORIGEN to the IAEA ORIGEN counts appears to be close. The percent difference between the count rates initially starts at ∼1.5%, peaks at a 14% difference shortly thereafter, and then drops again. Figures 3–5 provide more information on the short-lived and longer-lived isotopes that lead to this percent difference. These figures are generated by comparing count rate differences from decay constants, emission probabilities, and both at the same time. The nuclides are selected by tracking whichever nuclides have the largest absolute difference at each time step, as the shorter lived nuclides will have a smaller absolute difference as they decay away. Figure 3 shows that the peak decay constant difference causes around 1.2 million

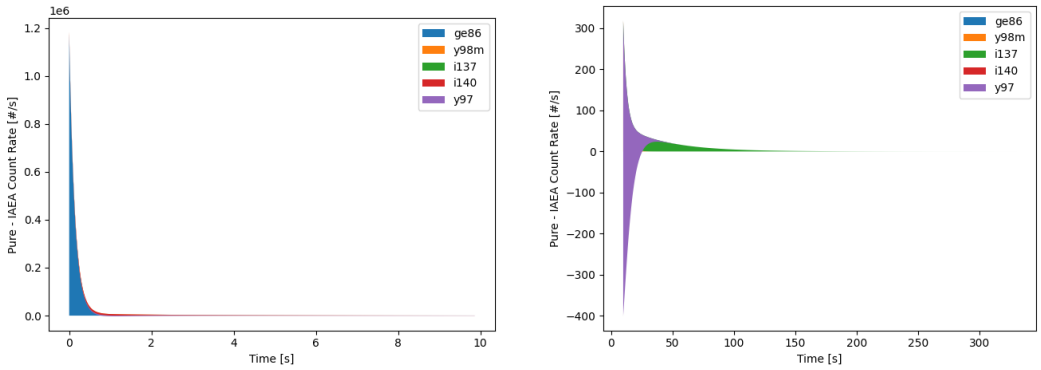

(a) Short time scale (b) Long time scale

Fig. 3. Decay constant–based difference between count rates with IAEA decay constants for ^{235}U fast-pulse irradiation over different time frames.

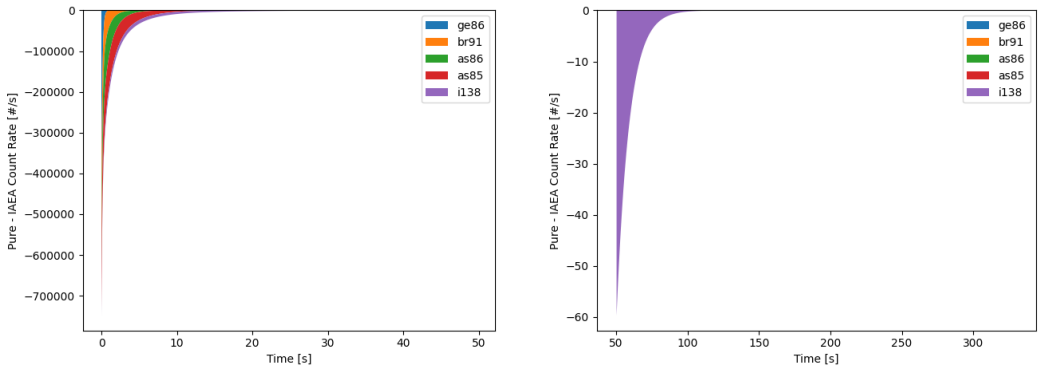

(a) Short time scale (b) Long time scale

Fig. 4. Emission probability (i.e., branching fraction)–based difference between count rates with IAEA decay constants for ^{235}U fast-pulse irradiation over different time frames.

counts per second, while the difference drops rapidly during later times. The emission probabilities have a smaller maximum effect, but the integral effect is larger; therefore, the combined effects of emission and decay constants are dominated by precursors that are significantly affected by emission probability data differences.

Table I lists the isotopes that have the most significant effect on the decay constant and emission probability data differences. Figures 4 and 5 show the impact these nuclides have on the delayed neutron count rate. From Table I, it can be seen that the emission probabilities affect the majority of the nuclides with the largest differences. These emission probability differences drive differences in the net yield as well. Table II shows the net yields from various data sets, and shows

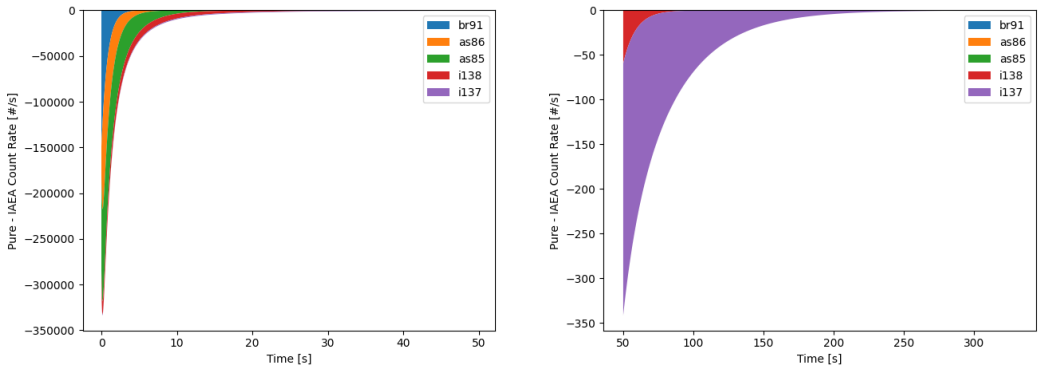

(a) Short time scale (b) Long time scale

Fig. 5. Combined decay constant and emission probability–based difference between count rates with IAEA decay constants for ^{235}U fast-pulse irradiation over different time frames.

TABLE I
Difference in data for isotopes with the largest difference in counts.

Isotope	$\lambda_{IAEA}\ [s^{-1}]$	$\lambda_{ORIGEN}\ [s^{-1}]$	$\Delta\lambda\ [s^{-1}]$	P_{IAEA}	P_{ORIGEN}	ΔP
^{91}Br	1.27	1.28	0.01	0.304	0.109	0.195
^{85}As	0.343	0.343	0.00	0.625	0.22	0.405
^{86}As	0.734	0.733	0.001	0.345	0.105	0.240
^{137}I	0.028	0.028	0.00	0.076	0.072	0.004
^{138}I	0.111	0.111	0.00	0.053	0.026	0.027
^{86}Ge	3.12	7.30	4.18	0.45	0.22	0.23
^{98m}Y	0.299	0.347	0.048	0.034	0.034	0.00
^{140}I	1.17	0.806	0.364	0.079	0.22	0.141
^{97}Y	0.185	0.185	0.00	5.8E-4	0.003	0.00242

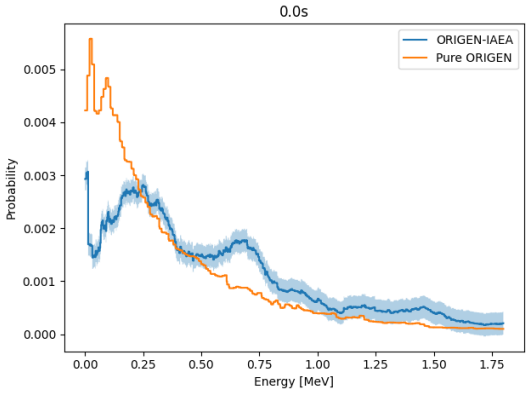

Fig. 6. Normalized difference in emission spectra of Pure ORIGEN and IAEA–ORIGEN for ^{235}U fast-pulse irradiation at 0 s.

that changing the decay constants does not largely impact the net yield while changing emission probabilities has an impact of approximately 200 pcm. This is because the net yield measures the total number of delayed neutrons, which means the time at which they are emitted is less important than the net number that are emitted.

Figure 6 shows how the initial spectra of the ORIGEN output compare to the IAEA–ORIGEN spectra immediately after irradiation. Although these results account for only one time step, the spectral differences become smaller over time, as shown in Figure 7. This discrepancy between the energy spectra shortly after irradiation aligns with the previously discussed results. Additionally, because the main differences occur in the first 2 s, the problematic isotopes can be determined directly. The results shown in Figures 3–5 indicate that those isotopes that differ most significantly within the first 2 s are ^{91}Br, ^{85}As, ^{86}As, ^{137}I, and ^{138}I.

III.B. Six Group Fits

The DNP six groups can be calculated using the generated delayed neutron count rate data and iterative least squares method. Recall from Section II that a detector efficiency, ϵ, of 3.75E-8 is used in all results to reflect the experimental results from Keepin, Wimett, and Zeigler [6].

Table II lists the net yield variance observed between the IAEA data and ORIGEN library data. Additionally, net yields from other works are shown for fast ^{235}U irradiation.

Emission probability is the principal reason yield varied between the IAEA data and the ORIGEN decay library; a shift in the decay constant data minimally affects the net yield. Additionally,

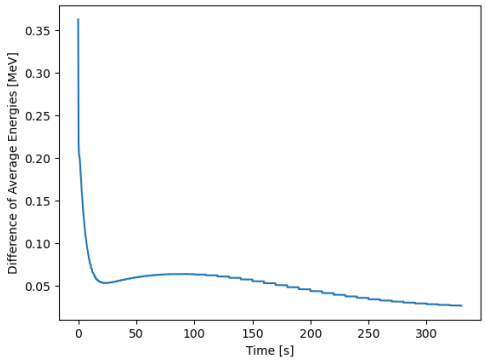

Fig. 7. Difference in average neutron energy of Pure ORIGEN and IAEA–ORIGEN for ^{235}U fast-pulse irradiation over time where Pure ORIGEN is subtracted from IAEA–ORIGEN.

TABLE II
Net delayed neutron yields from various sources of data (partially recreated from [11]).

λ	P_n	Yield
IAEA	IAEA	0.0191
ORIGEN	IAEA	0.0193
IAEA	ORIGEN	0.0172
ORIGEN	ORIGEN	0.0172
Keepin, Wimett, and Zeigler [6]	Keepin, Wimett, and Zeigler [6]	0.0165
Brady and England [11]	Brady and England [11]	0.0206
Tuttle [21]	Tuttle [21]	0.0167
ENDF/B-V [22]	ENDF/B-V [22]	0.0167
England et al. [23]	England et al. [23]	0.0198
England and Rider [24]	England and Rider [24]	0.0206

TABLE III
Six group fit half-life parameters given in seconds.

Fit	T_1	T_2	T_3	T_4	T_5	T_6
Brady and England [11]	52.1	21.2	5.74	2.29	0.816	0.243
Keepin, Wimett, and Zeigler [6]	54.5	21.8	6.00	2.23	0.496	0.179
IAEA	49.0	19.2	3.64	1.28	0.320	0.098
Pure	51.3	20.7	6.04	2.19	0.505	0.115

TABLE IV
Six group fit half-life parameters' uncertainties given in seconds.

Fit	ΔT_1	ΔT_2	ΔT_3	ΔT_4	ΔT_5	ΔT_6
Keepin, Wimett, and Zeigler [6]	0.94	0.54	0.17	0.06	0.03	0.02
IAEA	0.245	0.096	0.018	0.006	0.002	0.001
Pure	0.256	0.104	0.030	0.011	0.003	0.001

the net yields range from 0.0165 to 0.206 in the literature, which is a fairly large range of values. The current work's values fall within this range.

Tables III and V contain the group half-life and yield parameters, which were identified using the iterative least squares approach and the group fit parameters taken from Brady and England, referenced here since they are the parameters used in ENDF, and from Keepin, Wimett, and Zeigler [11, 6]. The uncertainties for the group fits are given in Tables IV and VI. An interesting note is that the IAEA group parameters are all smaller than all the other fits, which means that the delayed neutrons will overall be emitted more rapidly compared to the other fits.

For the group yields, the IAEA fit showed greater weight on the longer-lived groups, which is noticeable when comparing the longest- and shortest-lived group yields. A comparison of the fits is shown in Figure 8; this comparison indicates that the DNP group parameters in the current work are similar to other group parameters. The comparison also reveals discrepancies among the other referenced fits, although all of the fits shown are for the same fissile isotope and fast energy spectrum.

TABLE V
Six group fit yield parameters in delayed neutrons per fission multiplied by 100.

Fit	a_1	a_2	a_3	a_4	a_5	a_6
Brady and England [11]	0.072	0.372	0.355	0.797	0.327	0.137
Keepin, Wimett, and Zeigler [6]	0.063	0.351	0.310	0.672	0.211	0.043
IAEA	0.083	0.350	0.670	0.566	0.187	0.054
Pure	0.071	0.308	0.244	0.711	0.300	0.091

TABLE VI
Six group fit yield parameters' uncertainties in delayed neutrons per fission multiplied by 100.

Fit	Δa_1	Δa_2	Δa_3	Δa_4	Δa_5	Δa_6
Keepin, Wimett, and Zeigler [6]	0.005	0.011	0.028	0.023	0.015	0.005
IAEA	0.009	0.009	0.008	0.003	0.003	0.001
Pure	0.014	0.018	0.012	0.007	0.002	0.001

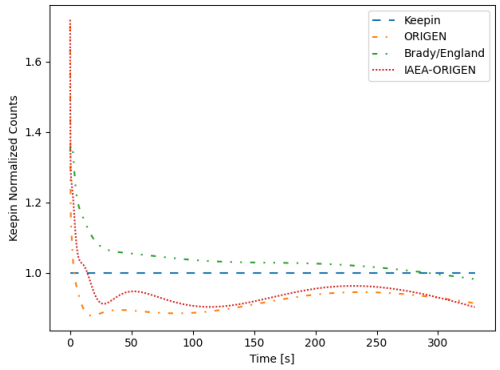

Fig. 8. A comparison of the different fast fission irradiation DNP six group fits of ^{235}U normalized to the Keepin, Wimett, and Zeigler six group fit count rate [6].

The discrepancies could be the result of differences in energy spectra causing fission, uncertainty in the number of fission events, uncertainty in the experimental data collected by Keepin, Wimett, and Zeigler (which were fitted), or uncertainty in the nuclear data used in the codes in this work and in Brady and England's work.

III.C. Six Group Spectra

Using the six group fits generated, as well as the energy-dependent count rate from ORIGEN and the constructed data from the IAEA database, the spectral profiles associated with each group can be generated, as shown in Equation (15). Figure 9 shows a comparison of the fractional fitting method and the iterative least squares method, labeled as data fit, implemented in this work. The figure shows the probability of a delayed neutron to be emitted in each bin with a width of $2\,keV$.

Figure 10 further compares the discrepancy between the historical fractional fitting approach and the proposed iterative least squares approach. The iterative least squares provided a much better fit than that of the fractional fitting method. This is shown specifically at 330 seconds, where the longer lived groups dominate the spectra.

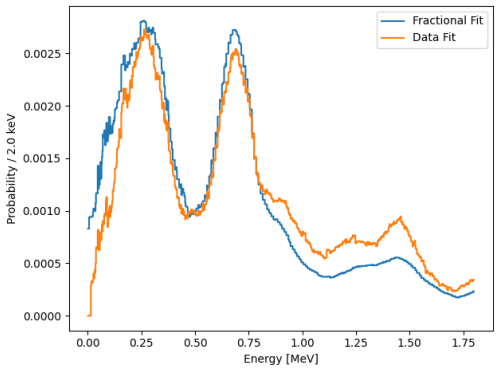

Fig. 9. Comparison of fractional fitting least squares method and iterative least squares method for the sixth precursor group for IAEA-ORIGEN in ^{235}U fast-pulse irradiation.

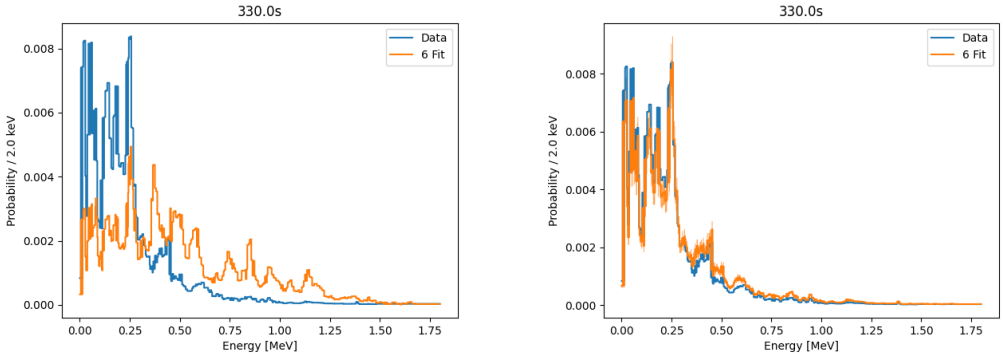

(a) Fractional fitting

(b) Iterative least squares

Fig. 10. Comparison of data with normalized IAEA-ORIGEN six group spectra for ^{235}U pulse irradiation at 330 seconds.

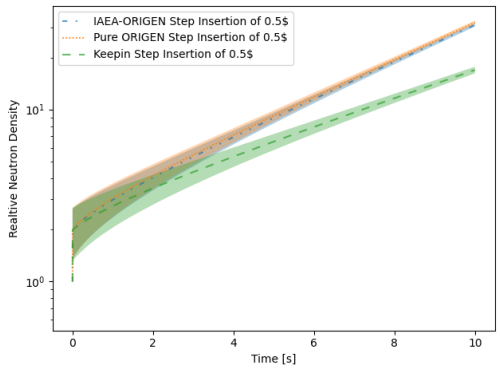

Fig. 11. Point reactor kinetic neutron density response to reactivity step insertion for different six group fits.

III.D. Point Reactor Kinetics Reactivity Insertion

To observe the effect of altering the group parameters, the response to a reactivity step insertion can be modeled using point reactor kinetics. In this problem, we use the following parameters: a neutron generation time of 0.1 μs, an average number of total neutrons per fission of 2.6, and the DNP group parameters from Section III.B. Figure 11 shows the neutron density response to a reactivity step insertion into a reactor with these parameters.

Figure 11 shows that the Keepin, Wimett, and Zeigler response was slightly lower than that of the current work [6]. The responses began closely aligned and diverged further apart as the effect of the DNPs becomes more significant. In the later times, the IAEA–ORIGEN neutron density was slightly lower than the Pure ORIGEN neutron density. This is because the group fit of Pure ORIGEN has higher yield values for five and six groups, the yield values of which dominate during the early times. This effect was counteracted slightly by the slightly longer lives of five and six groups that Pure ORIGEN also has, but the net effect was still an increased response compared with that of the IAEA–ORIGEN group fit. Following this logic, the Keepin, Wimett, and Zeigler group fit has small yields for five and six groups while also having fairly long half- lives for each group.

III.E. Westinghouse 17×17 Pressurized Water Reactor

Additional macroscopic analysis was conducted using SCALE/Polaris. SCALE/Polaris is a tool used to perform 2D lattice physics that provides six group kinetics parameters as an output.

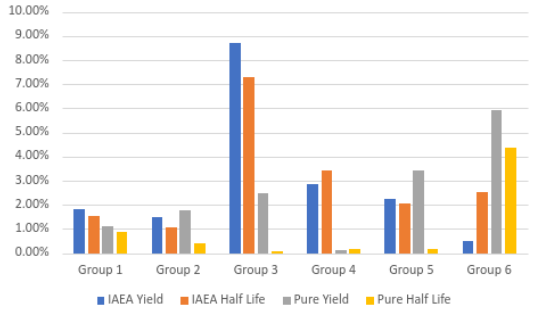

Fig. 12. The absolute percent difference of IAEA and Pure ORIGEN six group fits to the Keepin, Wimett, and Zeigler fits of fast spectrum ^{235}U in a Westinghouse 17×17 fuel assembly.

These outputs are importance weighted, nuclide integrated, and assembly homogenized. Because these kinetics parameters are used by other codes to perform transient analyses, it is important to determine the difference using the default kinetic parameters used as an input compared with the six group fits generated in this work.

For this analysis, only the fast-spectrum kinetics parameters were altered for ^{235}U. This adjustmented was performed to provide a conservative estimate for the magnitude of difference, which can be expected because of the heavily thermal spectrum.

The default values used for the kinetic parameter inputs are those from Keepin, Wimett, and Zeigler [6]. The IAEA and Pure ORIGEN six group fits presented in this work were then used. The resulting kinetics parameters outputs for each set of group fits were compared with the absolute percent differences shown in Figure 12.

These absolute percent differences from the Keepin, Wimett, and Zeigler data show that the largest difference in IAEA yield and half-life values was observed in the third precursor group; the greatest difference in those values for Pure ORIGEN was observed in the sixth precursor group. This result corresponds directly to the differences in the six group fits shown in Tables III and V.

IV. CONCLUSIONS AND FUTURE WORK

This work demonstrates generation of DNP group parameters from a simulated irradiation combined with data from the IAEA and from ORIGEN [1]. These group parameters use recent experimental data and propagated uncertainties to investigate the effects on reactor behavior. The results showed that some of the DNP data used in ORIGEN differs with the data from the IAEA database.

Specifically, a few particular nuclides have large differences between the IAEA database and in ORIGEN. The nuclides with the largest impact on the delayed neutron count rate following fast spectrum pulse irradiation of ^{235}U from data discrepancies include ^{91}Br, ^{85}As, ^{86}As, ^{137}I, ^{138}I, ^{86}Ge, ^{98m}Y, ^{140}I, and ^{97}Y. These discrepancies result in a 200 *pcm* difference in the total delayed neutron yield, as well as differences in the rate at which the delayed neutrons are emitted. The two sets of group parameters generated from this differing data in a point reactor kinetics model showed that the resulting neutron density responses are similar over a relatively short time period after large reactivity insertions. Discrepancies among the data between SOURCES4C and ENDF are currently being dealt with by relying more on ENDF and less on SOURCES4C where possible in SCALE.

The group spectra generation was also investigated in this work. The proposed method which allows each DNP to contribute to every DNP group showed promising results, providing a better fit than the fractional fitting method. The iterative least squares method proposed is more computationally expensive, but it is worthwhile provided the group spectra do not need to be regenerated frequently.

There are many different possible extensions which can further this work. Updates could be made to the group fits by implementing updated data and propagating uncertainty. The group spectra could also be updated with uncertainty propagation and methods for fitting optimal group spectra. A more thorough analysis of various group fitting methods for yields, abundances, and spectra could include using non-linear least squares or other least squares methods, calculating uncertainty when the decay constant mesh is refined to the furthest extent possible, and determining whether other methods would alter how many groups are needed for a fit within a given margin. Analysis of additional data sources, such as the Joint Evaluated Fission and Fusion library, could similarly identify additional isotopes causing discrepancies.

ACKNOWLEDGMENTS

This manuscript has been authored by UT-Battelle, LLC under contract DE-AC05-00OR22725 with the US Department of Energy (DOE). The US government retains and the publisher, by accepting the article for publication, acknowledges that the US government retains a nonexclusive, paid-up, irrevocable, worldwide license to publish or reproduce the published form of this

manuscript, or allow others to do so, for US government purposes. DOE will provide public access to these results of federally sponsored research in accordance with the DOE Public Access Plan (http://energy.gov/downloads/doe-public-access-plan). This material is based upon work supported under an Integrated University Program Graduate Fellowship. The authors are grateful for this generous support. Thanks to Friederike Bostelmann and Ugur Mertyurek for their review of this paper. Additional thanks to the University of Illinois Department of Nuclear, Plasma, and Radiological Engineering and the members of the Advanced Reactors and Fuel Cycles group for their support and suggestions in developing this work.

REFERENCES

[1] P. Dimitriou, I. Dillmann, B. Singh, V. Piksaikin, K. Rykaczewski, J. Tain, A. Algora, K. Banerjee, I. Borzov, D. Cano-Ott, S. Chiba, M. Fallot, D. Foligno, R. Grzywacz, X. Huang, T. Marketin, F. Minato, G. Mukherjee, B. Rasco, A. Sonzogni, M. Verpelli, A. Egorov, M. Estienne, L. Giot, D. Gremyachkin, M. Madurga, E. McCutchan, E. Mendoza, K. Mitrofanov, M. Narbonne, P. Romojaro, A. Sanchez-Caballero, and N. Scielzo, "Development of a Reference Database for Beta-Delayed Neutron Emission," Nuclear Data Sheets, **173**, 144 (2021); https://doi.org/10.1016/j.nds.2021.04.006., URL https://www.sciencedirect.com/science/article/pii/S0090375221000168, special Issue on Nuclear Reaction Data.

[2] D. Brown, M. Chadwick, R. Capote, A. Kahler, A. Trkov, M. Herman, A. Sonzogni, Y. Danon, A. Carlson, M. Dunn, D. Smith, G. Hale, G. Arbanas, R. Arcilla, C. Bates, B. Beck, B. Becker, F. Brown, R. Casperson, J. Conlin, D. Cullen, M.-A. Descalle, R. Firestone, T. Gaines, K. Guber, A. Hawari, J. Holmes, T. Johnson, T. Kawano, B. Kiedrowski, A. Koning, S. Kopecky, L. Leal, J. Lestone, C. Lubitz, J. Márquez Damián, C. Mattoon, E. McCutchan, S. Mughabghab, P. Navratil, D. Neudecker, G. Nobre, G. Noguere, M. Paris, M. Pigni, A. Plompen, B. Pritychenko, V. Pronyaev, D. Roubtsov, D. Rochman, P. Romano, P. Schillebeeckx, S. Simakov, M. Sin, I. Sirakov, B. Sleaford, V. Sobes, E. Soukhovitskii, I. Stetcu, P. Talou, I. Thompson, S. van der Marck, L. Welser-Sherrill, D. Wiarda, M. White, J. Wormald, R. Wright, M. Zerkle, G. Žerovnik, and Y. Zhu, "ENDF/B-VIII.0: The 8th Major Release of the Nuclear Reaction Data Library with CIELO-project Cross Sections, New Standards and Thermal Scattering Data," Nuclear Data Sheets, **148**, 1 (2018); https://doi.org/10.1016/j.nds.2018.02.001., URL https://www.sciencedirect.com/science/article/pii/S0090375218300206, special Issue on Nuclear Reaction Data.

[3] T. Parish, W. Charlton, N. Shinohara, M. Andoh, M. Brady, and S. Raman, "Status of six-group delayed neutron data and relationships between delayed neutron parameters from

the macroscopic and microscopic approaches," Nuclear science and engineering, **131**, 2, 208 (1999).

[4] M. Chadwick, P. Obložinský, M. Herman, N. Greene, R. McKnight, D. Smith, P. Young, R. MacFarlane, G. Hale, S. Frankle, A. Kahler, T. Kawano, R. Little, D. Madland, P. Moller, R. Mosteller, P. Page, P. Talou, H. Trellue, M. White, W. Wilson, R. Arcilla, C. Dunford, S. Mughabghab, B. Pritychenko, D. Rochman, A. Sonzogni, C. Lubitz, T. Trumbull, J. Weinman, D. Brown, D. Cullen, D. Heinrichs, D. McNabb, H. Derrien, M. Dunn, N. Larson, L. Leal, A. Carlson, R. Block, J. Briggs, E. Cheng, H. Huria, M. Zerkle, K. Kozier, A. Courcelle, V. Pronyaev, and S. van der Marck, "ENDF/B-VII.0: Next Generation Evaluated Nuclear Data Library for Nuclear Science and Technology," Nuclear Data Sheets, **107**, 12, 2931 (2006); https://doi.org/10.1016/j.nds.2006.11.001., URL https://www.sciencedirect.com/science/article/pii/S0090375206000871, evaluated Nuclear Data File ENDF/B-VII.0.

[5] M. C. Brady, "Evaluation and application of delayed neutron precursor data," PhD Thesis, Texas A&M University (1988).

[6] G. Keepin, T. Wimett, and R. Zeigler, "Delayed neutrons from fissionable isotopes of uranium, plutonium and thorium," Journal of Nuclear Energy (1954), **6**, 1, IN2 (1957); https://doi.org/10.1016/0891-3919(57)90178-X., URL https://www.sciencedirect.com/science/article/pii/089139195790178X.

[7] D. J. Hughes, J. Dabbs, A. Cahn, and D. Hall, "Delayed Neutrons from Fission of U^{235}," Phys. Rev., **73**, 111 (1948); 10.1103/PhysRev.73.111., URL https://link.aps.org/doi/10.1103/PhysRev.73.111.

[8] D. J. Loaiza, G. Brunson, R. Sanchez, and K. Butterfield, "Measurements of Absolute Delayed Neutron Yield and Group Constants in the Fast Fission of 235U and 237Np," Nuclear Science and Engineering, **128**, 3, 270 (1998); 10.13182/NSE98-A1955., URL https://doi.org/10.13182/NSE98-A1955.

[9] D. J. Loaiza and F. E. Haskin, "Dominant Delayed Neutron Precursors to Model Reactivity Predictions for Multiple Fissioning Nuclides," Nuclear Science and Engineering, **134**, 1, 22 (2000); 10.13182/NSE00-A2097., URL https://doi.org/10.13182/NSE00-A2097.

[10] D. Saphier, D. Ilberg, S. Shalev, and S. Yiftah, "Evaluated Delayed Neutron Spectra and Their Importance in Reactor Calculations," Nuclear Science and Engineering, **62**, 4, 660 (1977); 10.13182/NSE77-A15209., URL https://doi.org/10.13182/NSE77-A15209.

[11] M. C. Brady and T. R. England, "Delayed Neutron Data and Group Parameters for 43 Fissioning Systems," Nuclear Science and Engineering, **103**, 2, 129 (1989); 10.13182/NSE103-129., URL https://doi.org/10.13182/NSE103-129.

[12] G. Rudstam, "Six-Group Representation of the Energy Spectra of Delayed Neutrons from Fission," Nuclear Science and Engineering, **80**, 2, 238 (1982); 10.13182/NSE82-A21428., URL https://doi.org/10.13182/NSE82-A21428.

[13] T. R. England, W. B. Wilson, R. E. Schenter, and F. M. Mann, "Aggregate Delayed Neutron Intensities and Spectra Using Augmented ENDF/B-V Precursor Data," Nuclear Science and Engineering, **85**, 2, 139 (1983); 10.13182/NSE83-A27422., URL https://doi.org/10.13182/NSE83-A27422.

[14] W. Wieselquist and R. A. Lefebvre, "SCALE 6.3.1 User Manual," ORNL/TM-SCALE-6.3.1, Oak Ridge National Laboratory (ORNL), Oak Ridge, TN (United States) (2023); 10.2172/1959594., URL https://www.osti.gov/biblio/1959594.

[15] R. E. Peterson and G. A. Newby, "AN UNREFLECTED U-235 CRITICAL ASSEMBLY," Nuclear Science and Engineering, **1**, 112 (1956)URL https://api.semanticscholar.org/CorpusID:123304404.

[16] W. B. Wilson, R. T. Perry, W. Charlton, T. Parish, and E. Shores, "SOURCES: a code for calculating (α, n), spontaneous fission, and delayed neutron sources and spectra," Radiation protection dosimetry, **115**, 1-4, 117 (2005).

[17] J. K. Tuli et al., "Evaluated nuclear structure data file," A Manual for Preparation of Data Sets-National Nuclear Data Center Brookhaven National Laboratory PO Box, **5000**, 11973 (2001).

[18] C. Tofallis, "Least squares percentage regression," Journal of Modern Applied Statistical Methods (2009).

[19] C. L. Lawson and R. J. Hanson, Solving least squares problems, SIAM (1995).

[20] M. I. Radaideh, W. A. Wieselquist, and T. Kozlowski, "A new framework for sampling-based uncertainty quantification of the six-group reactor kinetic parameters," Annals of Nuclear Energy, **127**, 1 (2019).

[21] R. Tuttle, "Delayed-neutron yields in nuclear fission," Proc. Second Consultants Meeting on Delayed Neutron Properties, vol. 29 (1979).

[22] R. Kinsey, L. Stewart, R. LaBauve, P. Young, A. Horsley, G. Hale, M. Battat, H. Perkins, C. Cowan, C. Fu, F. Perey, D. Foster, B. Magurno, D. Larson, M. Allen, M. Drake, C. Philis, A. Smith, R. Howerton, F. Mann, A. Prince, T. Burrows, S. Mughabghab, M. Divadeenam, R. Howerton, M. Bhat, H. Takahashi, B. Leonard, K. Stewart, D. Sargis, T. Maung, J. Otter, C. Dunford, E. Ottewitte, W. Henderson, J. Zwick, E. Kujawski, L. Weston, and R. Wright, "ENDF/B Summary Documentation," , Brookhaven National Laboratory (1979).

[23] W. Wilson, T. England, R. Schenter, and F. Mann, "Delayed neutron study using ENDF/B-VI basic nuclear data," Progress in Nuclear Energy, **41**, 1, 71 (2002); https://doi.org/10.1016/S0149-1970(02)00006-9., URL https://www.sciencedirect.com/science/article/pii/S0149197002000069.

[24] T. R. England and B. F. Rider, "Status of fission yield evaluations," , Los Alamos National Laboratory (LANL), Los Alamos, NM (United States) (1983); 10.2172/5509379., URL https://www.osti.gov/biblio/5509379.